Cellular Finite Beam Element for Nonlinear Analysis of Concrete Structures under Fire

Fabio Biondini, M. ASCE[1]; and Andrea Nero[2]

Abstract: A novel approach to nonlinear finite-element analysis of concrete structures exposed to fire is presented. The proposed formulation refers to frame systems, but it can be extended to other types of structures. The main novelty of this formulation is the use of a special class of evolutionary algorithms, known as cellular automata, to describe the heat transfer process induced by fire and to create an effective link between the simulation of the thermal process and the structural analysis. The heat transfer process is reproduced by considering heat conduction, heat convection, and thermal radiation. The temperature effects on the structural performance are taken into account by means of temperature-dependent thermal and mechanical properties of concrete and steel. In this way, the general criteria for nonlinear finite-element analysis of concrete structures are applied to formulate a cellular reinforced concrete beam element with temperature-dependent characteristics. The effectiveness and applicability in engineering practice of the proposed formulation is demonstrated through applications. The results prove the accuracy of the proposed procedure and show that, for statically indeterminate structures, fire safety needs to be evaluated at the global level by taking into account the actual role played by the structural scheme. **DOI: 10.1061/(ASCE)ST.1943-541X.0000307.**

CE Database subject headings: Concrete structures; Finite element method; Fire resistance; Heat transfer; Nonlinear analysis.

Introduction

In structural design, approximate methods are applied to assess the structural performance of reinforced concrete cross sections or members under fire [Hertz 1985; European Committee for Standardization (CEN) 2004; American Concrete Institute (ACI)/Minerals, Metals and Materials Society (TMS) 2007]. This approach can provide useful information at a preliminary design stage, and can be easily applied for statically determinate structures. However, particularly for statically indeterminate systems, accurate fire simulations by means of time-variant nonlinear analysis procedures are often required to properly address the choices involved in the design of new structures, and in the rehabilitation of the existing ones, to achieve the required level of fire performance and safety.

Several fire-dedicated computational tools based on finite-element or finite-difference methods have been proposed in the literature, including computer programs such as FIRE-RC (Becker and Bresler 1974), FIRES-T3 (Iding et al. 1977), CONFIRE (Forsén 1982), TASEF (Sterner and Wickström 1990), TEMPCALC (Anderberg 1991), and SAFIR (Franssen et al. 2000). The standard computational approach is to perform a thermal fire analysis and use the temperature maps in a separate finite-element program to evaluate the temperature-dependent structural performance. Finite-element procedures have also been proposed to investigate the effects of fire-induced spalling that may occur for low permeability concrete materials, such as high-strength concrete or shotcrete (Caner et al. 2005; Pichler et al. 2006; Kodur and Dwaikat 2008).

The aim of this paper is to present a novel integrated approach to thermomechanical nonlinear finite-element analysis of concrete structures exposed to fire (Biondini and Nero 2006). The attention is focused on normal strength concrete frame systems, but the proposed formulation can be specialized to other types of concrete materials and structures. The main novelty of this formulation is the use of a special class of evolutionary algorithms, known as cellular automata, to describe the heat transfer process induced by fire and to create an effective link between the simulation of the thermal process and the structural analysis. This link makes the proposed approach more general than other procedures in which thermal and structural analyses are uncoupled. In fact, although the thermal properties of concrete are generally assumed to be independent from the stress state (CEN 2004), in some cases the occurrence of stress-related damage phenomena, such as severe cracking, may modify the temperature distribution and lead to a coupling between heat transfer and structural response.

Recently, cellular automata have been successfully applied to simulate the diffusion processes involved in durability analysis of concrete structures (Biondini et al. 2004). The algorithm proposed in this paper starts from similar criteria. However, its formulation has been extended to accurately reproduce not only the internal diffusive flow associated with heat conduction, but also the external thermal flow due to heat convection and thermal radiation.

On the basis of this evolutionary model, temperature effects on the structural performance are evaluated by introducing temperature-dependent laws for both the thermal and mechanical properties of the component materials, concrete and steel, and by taking into account the additional deformative effects induced by heat transfer. In this way, the coupling between thermal process and structural behavior leads to the cellular automata formulation of a deteriorating reinforced concrete finite beam element for the time-variant nonlinear structural analysis under fire.

[1]Dept. of Structural Engineering, Politecnico di Milano Piazza L. da Vinci, 32 20133 Milan, Italy (corresponding author). E-mail: biondini@stru.polimi.it

[2]Tecnomare S.p.A Via Enrico Caviglia, 11 20139 Milan, Italy. E-mail: andrea.nero@tecnomare.it

Note. This manuscript was submitted on December 18, 2008; approved on August 23, 2010; published online on August 25, 2010. Discussion period open until October 1, 2011; separate discussions must be submitted for individual papers. This paper is part of the ***Journal of Structural Engineering***, Vol. 137, No. 5, May 1, 2011. ©ASCE, ISSN 0733-9445/2011/5-543–558/$25.00.

The effectiveness and applicability in engineering practice of the proposed methodology is demonstrated through applications (Biondini and Nero 2006, 2007). The obtained results prove the accuracy of the proposed procedure and show that for statically indeterminate structures, fire safety needs to be evaluated at the global level by taking into account the actual role played by the structural scheme.

Modeling of Heat Transfer

Heat transfer is the energy transmission process that involves objects having different temperatures. There are primarily three distinct ways of heat transfer: heat conduction, heat convection, and thermal radiation. In fire structural engineering, all such transmission methods can play an important role (Buchanan 2001). For this reason, an accurate modeling of heat transfer must account for conduction into solid bodies and for convection and radiation between the solid body and the outer heating sources.

Heat Conduction

The conduction of heat in solids is usually described by the Fourier model, which, for isotropic media and in absence of internal sources of heat, is represented by the following second order partial differential nonlinear equation (Incropera and De Witt 2002):

$$\nabla(\lambda \nabla T) = c\rho \frac{\partial T}{\partial t} \tag{1}$$

where $T = T(\mathbf{x}, t)$ = temperature at point $\mathbf{x} = (x, y, z)$ and time t; $\lambda = \lambda(\mathbf{x}, T)$ = thermal conductivity; $c = c(\mathbf{x}, T)$ = specific heat; $\rho = \rho(\mathbf{x}, T)$ = material density; and $\nabla T = \mathbf{grad}\, T$. If the thermal conductivity λ does not depend on position $\mathbf{x}$, the previous differential equation simplifies in the following form:

$$D\nabla^2 T = \frac{\partial T}{\partial t} \tag{2}$$

where $D = D(\mathbf{x}, T) = \lambda/(c\rho)$ = thermal diffusivity; and $\nabla^2 = \nabla \cdot \nabla$. If the thermal diffusivity D does not depend on temperature T, the previous differential equation is linear. However, the thermal properties of concrete strongly depend on temperature, as shown in Fig. 1 (CEN 2004), where for the conductivity λ the lower limit is usually assumed. Therefore, the heat conduction process in reinforced concrete structures exposed to fire is generally nonlinear.

The thermal properties shown in Fig. 1 refer to normal strength concrete. The effects of temperature on thermal properties of high-strength concrete are investigated in Kodur and Sultan (2003). The thermal properties of steel are not considered in the proposed approach because the effects of reinforcement are usually negligible in the heat transfer process.

Heat Convection and Thermal Radiation

The heat flow $q = q(\mathbf{x}_s, t)$ prescribed at the surface point $\mathbf{x}_s$ of the solid body may be decomposed into two contributions, $q_c = q_c(\mathbf{x}_s, t)$ and $q_r = q_r(\mathbf{x}_s, t)$, owing to heat convection and thermal radiation, respectively:

$$q = q_c + q_r \tag{3}$$

Heat convection is a thermal phenomenon in which heat flow is generated in consequence of macroscopic movements of a fluid

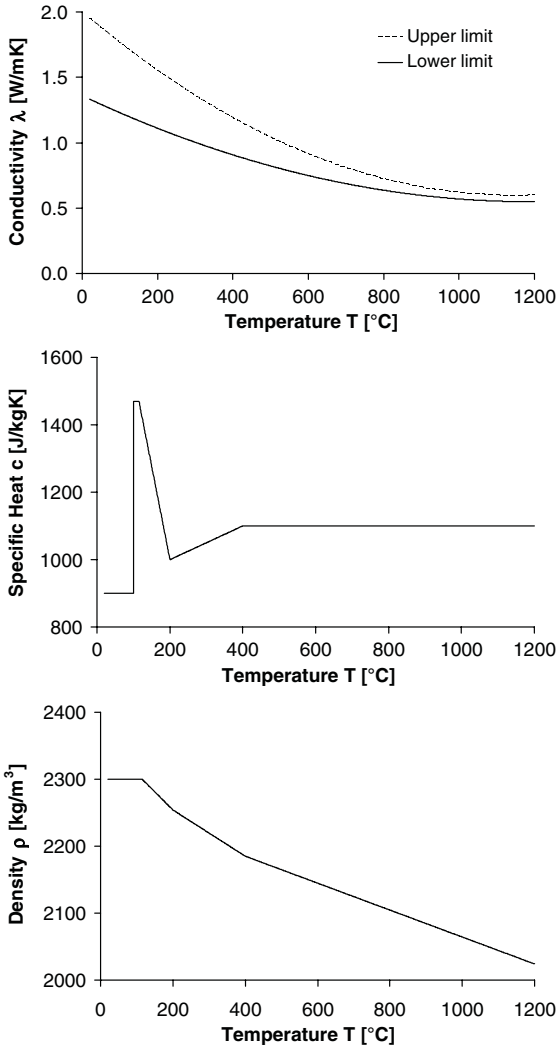

Fig. 1. Thermal properties of concrete (moisture content of 1.5%)

system. In general, the analytical description of a convection process is very complex. For this reason, heat convection is usually modeled by using empirical formulations. Newton's law of cooling (Incropera and De Witt 2002) is adopted in this study:

$$q_c = h(T_c - T) \tag{4}$$

where $T_c = T_c(t)$ = temperature of the convective medium; $T = T(\mathbf{x}_s, t)$ = temperature of the solid surface; and $h = h(\mathbf{x}_s, T)$ = convection coefficient.

Thermal radiation is the transmission of heat flow from an object in virtue of its temperature, without any mass transfer. Based on the Stefan-Boltzmann law, the radiative heat flow between two gray surfaces can be evaluated as follows (Incropera and De Witt 2002):

$$q_r = b(T_r^4 - T^4) \tag{5}$$

where $T_r = T_r(t)$ = temperature of the radiative body; $b = b(\mathbf{x}_s, t) = \sigma_n \varepsilon_r \varphi$ = radiation coefficient; σ_n = Boltzmann constant; $\varepsilon_r = \varepsilon_r(\mathbf{x}_s, T)$ = emissivity coefficient; and $\varphi = \varphi(\mathbf{x}_s)$ = view factor.

Cellular Automata Solution of the Heat Transfer Equations

Cellular automata represent simple mathematical idealizations of physical systems in which space and time are discrete, and physical quantities take on a finite set of discrete values (Wolfram 1994). In its basic form, a cellular automaton consists of a regular uniform grid of sites or cells, theoretically having infinite extension, with a discrete variable in each cell that can take on a finite number of states. The state at time t of the cellular automaton is then completely defined by the values of the variable $s_i = s_i(t)$ at each cell i. During time, cellular automata evolve in discrete time steps according to a parallel state transition determined by a set of local rules: the variables $s_i^{k+1} = s_i(t_{k+1})$ at each site i at time t_{k+1} are updated synchronously based on the values of the variables s_n^k in their "neighborhood" n at the preceding time instant t_k. The neighborhood n of a cell i is typically taken to be the cell itself and a set of adjacent cells within a given radius r, or $(i-r) \le n \le (i+r)$. Thus, the dynamics of a cellular automaton can be formally represented as

$$s_i^{k+1} = \phi(s_n^k), \qquad i - r \le n \le i + r \tag{6}$$

where ϕ = evolutionary rule of the automaton. Clearly, a proper choice of the neighborhood plays a crucial role in determining the effectiveness of such rule. Fig. 2 shows an example of typical neighborhoods for one- and two-dimensional cellular automata, but patterns of higher complexity can also be proposed. Special attention is due to neighborhoods along the sides of the finite grid, for which the evolutionary rule should be defined according to the imposed boundary conditions.

In general, any physical system satisfying differential equations may be modeled as a cellular automaton. In particular, it can be shown that the heat transfer process in d-dimensions ($d = 1$, 2, 3) can be effectively simulated by adopting a von Neumann neighborhood with radius $r = 1$ and the following evolutionary rule (Biondini and Nero 2006):

$$T_i^{k+1} = \phi_{i,0} T_i^k + \sum_{j=1}^{d} (\phi_{i,j}^- T_{i-1,j}^k + \phi_{i,j}^+ T_{i+1,j}^k) \tag{7}$$

where the discrete variable $s_i^k = T_i^k = T(\mathbf{x}_i, t_k)$ represents the temperature of the cell i at time t_k, and the value of the evolutionary coefficients $\phi_{i,0}$ and $\phi_{i,j}^{\pm}$ depends on the nature of the neighborhood cells $(i \pm 1, j)$.

If the cells $(i \pm 1, j)$ are associated with a fire source, represented by convective fluids and radiative bodies, the corresponding evolutionary coefficients $\phi_{i,j}^{\pm}$ can be set as follows:

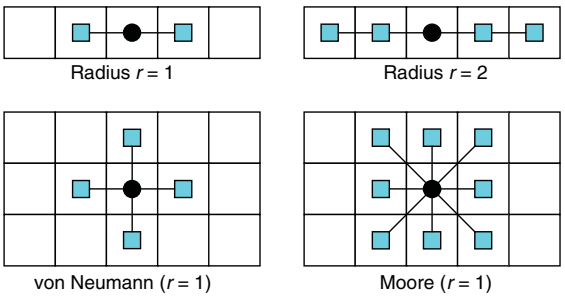

Fig. 2. Typical neighborhoods for one- and two-dimensional cellular automata

$$\phi_{i,j}^{\pm} = F_i (B_{i,j}^{\pm} + R_{i,j}^{\pm}) \tag{8}$$

where the dimensionless factors F_i (Fourier number), $B_{i,j}^{\pm}$ (Biot number), and $R_{i,j}^{\pm}$ (Radiation number), represent the contribution of heat conduction, heat convection, and thermal radiation, respectively. For a cellular automaton defined by a grid dimension Δx and a time step Δt, such contributions are related to the thermal properties of the cell i and to both the convective and radiative characteristics of the cells $(i \pm 1, j)$, in the following way:

$$F_i = \frac{\lambda_i \Delta t}{c_i \rho_i \Delta x^2} = \frac{D_i \Delta t}{\Delta x^2} \tag{9}$$

$$B_{i,j}^{\pm} = \frac{h_{i\pm1,j} \Delta x}{\lambda_i} \tag{10}$$

$$R_{i,j}^{\pm} = \frac{b_{i\pm1,j} \Delta x}{\lambda_i} T_{i\pm1,j}^{k^3} \tag{11}$$

Conversely, if the cells $(i \pm 1, j)$ are not associated with a fire source, the evolutionary coefficients $\phi_{i,j}^{\pm}$ simplify as follows:

$$\phi_{i,j}^{\pm} = F_{i,j}^{\pm} = \frac{\lambda_{i,j}^{\pm} \Delta t}{c_i \rho_i \Delta x^2} = \frac{D_{i,j}^{\pm} \Delta t}{\Delta x^2} \tag{12}$$

where the following nonlocal definition of equivalent thermal conductivities $\lambda_{i,j}^{\pm}$ of the cell i is introduced:

$$\lambda_{i,j}^{\pm} = 2 \left(\frac{1}{\lambda_i} + \frac{1}{\lambda_{i\pm1,j}} \right)^{-1} \tag{13}$$

Finally, based on the continuity principle, the central evolutionary coefficient $\phi_{i,0}$ is obtained:

$$\phi_{i,0} = 1 - \left[\psi + \sum_{j=1}^{d} (\phi_{i,j}^- + \phi_{i,j}^+) \right] \tag{14}$$

where the coefficient ψ represents the eventual nonlinear supply of the radiative thermal flow:

$$\psi = \sum_{j=1}^{d} [\Delta \phi_{i,j}^- + \Delta \phi_{i,j}^+] \tag{15}$$

with

$$\Delta \phi_{i,j}^{\pm} = \Delta R_{i,j}^{\pm} = \frac{b_{i\pm1,j} \Delta x}{\lambda_i} (T_i^{k^3} - T_{i\pm1,j}^{k^3}) \tag{16}$$

when the cells $(i \pm 1, j)$ are associated with a radiative source, and $\Delta \phi_{i,j}^{\pm} = 0$ otherwise.

Clearly, a proper balance between grid dimension Δx and time step Δt must be achieved consistently with the required level of accuracy. To this aim, a suitable discretization in space and time may be chosen with reference to the case of homogeneous and isotropic solid medium, which usually characterizes the problem

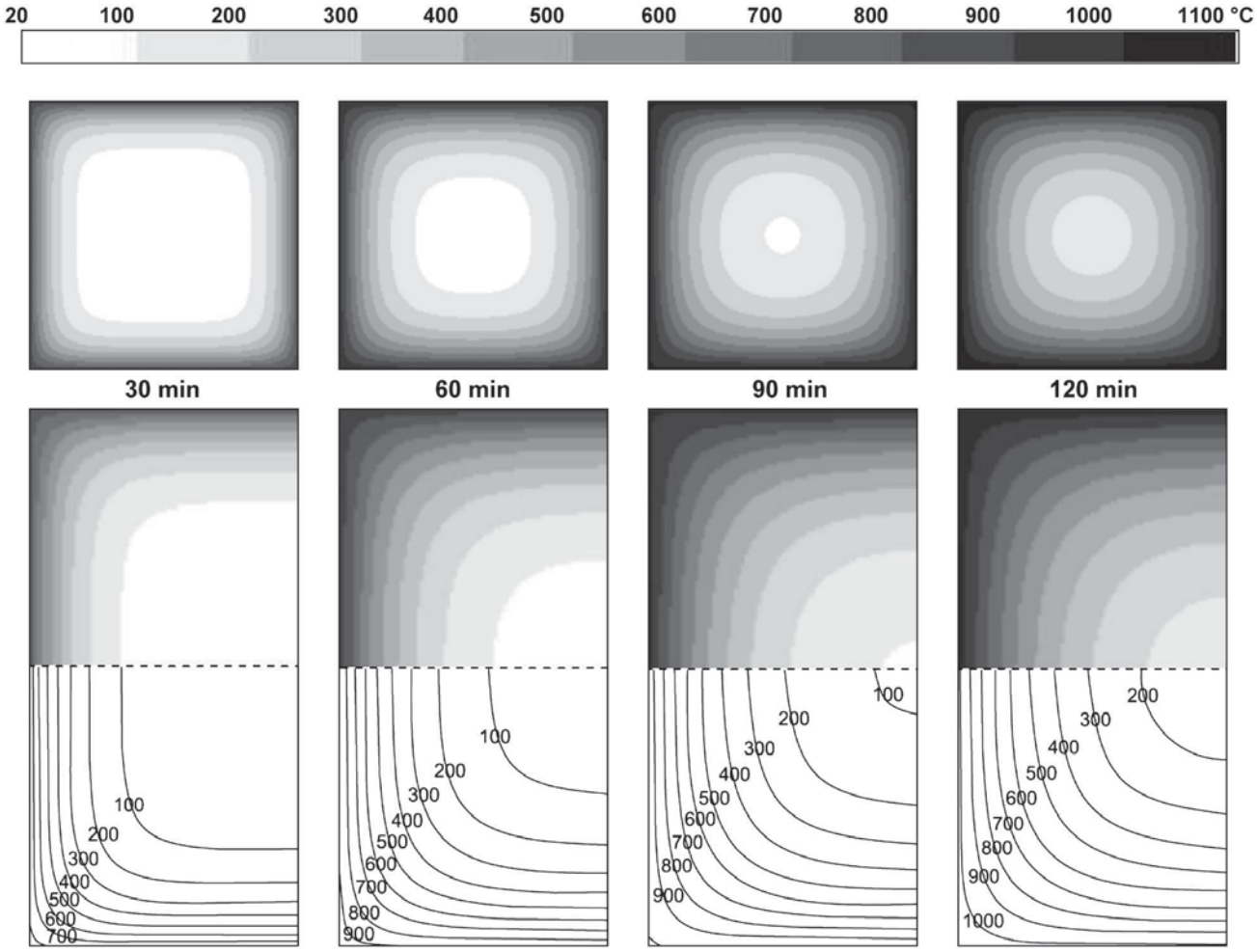

Fig. 3. Time-evolution of the temperature maps for a 300×300 mm concrete cross section subjected to a standardized fire ISO 834 (ISO 1975) along the boundary surface (thermal properties of Fig. 1, with $h = 25$ kW/m^2 and $b = 0.7\sigma_n$), comparison between the grayscale results provided by a cellular automata simulation ($\Delta x = 1.874$ mm; $\Delta t = 0.01$ min) and the contour maps given in CEN (2004)

at the initial time $t = 0$. In such cases, the symmetry condition $\phi_{i,j}^- = \phi_{i,j}^+ = \phi_{i,1} \equiv \phi_1 (j = 1, \ldots, d)$ must hold for each cell i, with $\phi_{i0} \equiv \phi_0 = (1 - 2d\phi_1)$. Therefore, after the initial value of the evolutionary coefficients ϕ_0 and ϕ_1 is properly fixed, a consistent value of both grid dimension Δx and time step Δt is chosen to regulate the process according to a given reference value of the thermal diffusivity D:

$$D = \frac{1 - \phi_0}{2d} \frac{\Delta x^2}{\Delta t} = \phi_1 \frac{\Delta x^2}{\Delta t} \tag{17}$$

Suitable initial values of the evolutionary coefficients are $\phi_0 = 1/2$ and $\phi_1 = 1/(4d)$.

Validation of the Cellular Automata Solution

The cellular automata solution of the heat transfer equations has been successfully validated for one-, two-, and three-dimensional problems (Nero 2006). Temperature maps for cross sections exposed to fire are available in CEN (2004) and ACI/TMS (2007). As an example, Fig. 3 shows the time-evolution of the temperature maps for a 300×300 mm concrete cross section subjected to a standardized fire ISO 834 (ISO 1975) along the boundary surface. The comparison presented in Fig. 3 between the results of a cellular automata simulation and those provided in CEN (2004) proves the high accuracy of the proposed numerical model.

Constitutive Laws of Materials

The effects of high temperatures on material behavior usually involve remarkable strength reductions and the onset of a temperature-induced strain ε_T in addition to the stress-induced strain ε_σ, or $\varepsilon = \varepsilon_\sigma + \varepsilon_T$, for both concrete and steel.

Concrete Behavior

The instantaneous stress-induced strain ε_σ in compression is modeled by using the Schneider's stress-strain constitutive law (CEN 2004; Schneider 1988):

$$\frac{\sigma}{f_{c,T}} = \frac{n(\varepsilon_\sigma / \varepsilon_{c1,T})}{(n-1) + (\varepsilon_\sigma / \varepsilon_{c1,T})^n}, \qquad \varepsilon_\sigma \le \varepsilon_{cu,T} \tag{18}$$

where $\varepsilon_{c1,T}$ = peak strain associated with the compression strength $f_{c,T}$ at the temperature T; $\varepsilon_{cu,T}$ = corresponding ultimate strain; and $n = 3$. The thermal degradation of concrete properties depends on the stress level (ACI/TMS 2007). This dependency is particularly

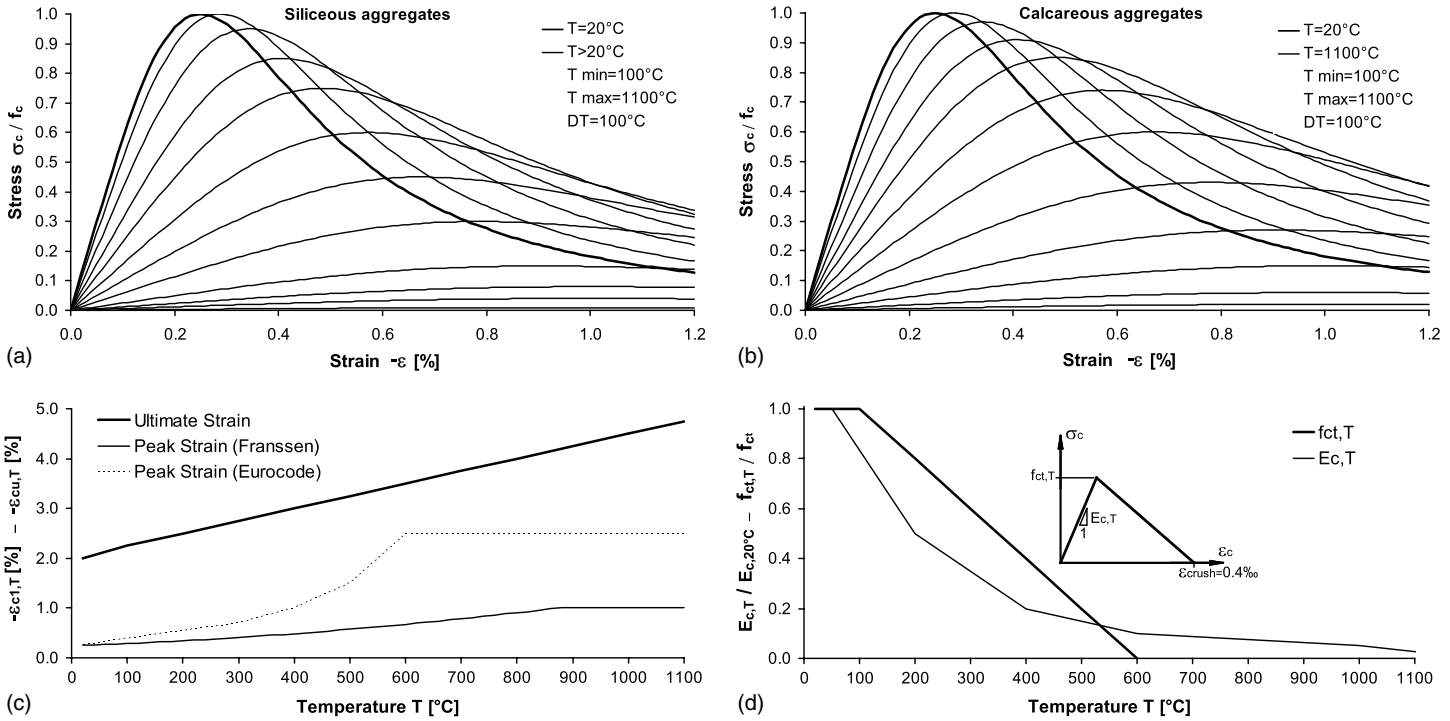

Fig. 4. Temperature-dependent concrete behavior. Stress-strain relationships in compression for (a) siliceous aggregates and (b) calcareous aggregates; (c) peak and ultimate strains in compression; (d) strength and elastic modulus in tension

relevant for structures loaded in the elastic range with a stress ratio $\sigma/f_{c,20} \leq 0.3$ (Schneider et al. 2008), where $f_{c,20}$ is the compression strength at the initial temperature $T = 20$°C. Although the dependency of thermal degradation on the loading history can easily be implemented in the proposed formulation according to CEN (2004), a constitutive model independent from the stress level is considered in this study. Figs. 4(a) and 4(b) show the evolution with temperature of the compression stress-strain law for concrete with siliceous and calcareous aggregates, respectively. The values of compression strength $f_{c,T}$ and ultimate strain $\varepsilon_{cu,T}$ are assumed consistently with CEN (2004). Peak strain is instead evaluated according to the following relationship (Franssen 1987):

$$\varepsilon_{c1,T} = 2.5 \times 10^{-3} + 4.1 \times 10^{-6}(T-20) + 5.5 \times 10^{-9}(T-20)^2 \leq 10^{-2} \tag{19}$$

In fact, the values of $\varepsilon_{c1,T}$ provided in CEN (2004) are overestimated to implicitly include, in an approximated way, the transient strain component of the temperature-induced strain ε_T in the stress-induced strain ε_σ [Fig. 4(c)]. For the stress-induced strain ε_σ in tension, the bilinear model shown in Fig. 4(d) is adopted (Rigberth 2000).

The temperature-induced strain ε_T is due to the contribution of three terms: thermal strain ε_{th}, transient strain ε_{tr}, and creep strain ε_{cr}, or $\varepsilon_T = \varepsilon_{th} + \varepsilon_{tr} + \varepsilon_{cr}$. According to CEN (2004), the thermal strain ε_{th} is given by the following relationships, for both siliceous aggregates:

$$\varepsilon_{th} = -1.8 \times 10^{-4} + 9 \times 10^{-6}T + 2.3 \times 10^{-11}T^3, \quad \text{for } 20\text{°C} \leq T \leq 700\text{°C} \tag{20a}$$

$$\varepsilon_{th} = 14 \times 10^{-3}, \quad \text{for } 700\text{°C} < T \leq 1200\text{°C} \tag{20b}$$

and calcareous aggregates:

$$\varepsilon_{th} = -1.2 \times 10^{-4} + 6 \times 10^{-6}T + 1.4 \times 10^{-11}T^3, \quad \text{for } 20\text{°C} \leq T \leq 805\text{°C} \tag{21a}$$

$$\varepsilon_{th} = 12 \times 10^{-3}, \quad \text{for } 805\text{°C} < T \leq 1200\text{°C} \tag{21b}$$

Transient strain ε_{tr} and creep strain ε_{cr} are evaluated according to the formulations proposed by Anderberg and Thelandersson (1976). The transient strain ε_{tr} is considered to be proportional to the thermal strain ε_{th} and to the ratio between actual stress σ and compression strength $f_{c,20}$ at the initial temperature $T = 20$°C:

$$\varepsilon_{tr} = -2.35\frac{\sigma}{f_{c,20}}\varepsilon_{th} \tag{22}$$

The contribution $\Delta\varepsilon_{cr}$ to creep strain ε_{cr} depends instead on the ratio between actual stress σ and compression strength $f_{c,T}$ at temperature $T > 20$°C:

$$\Delta\varepsilon_{cr} = -530 \times 10^{-6}\frac{\sigma}{f_{c,T}}\sqrt{\frac{\Delta t}{3}}e^{3.04(T-20)/1000} \tag{23}$$

where Δt (h) = reference time interval. Such contribution is particularly important with sustained high temperatures and in the evaluation of the time-dependent deflections during the cooling phase (Hertz 1985).

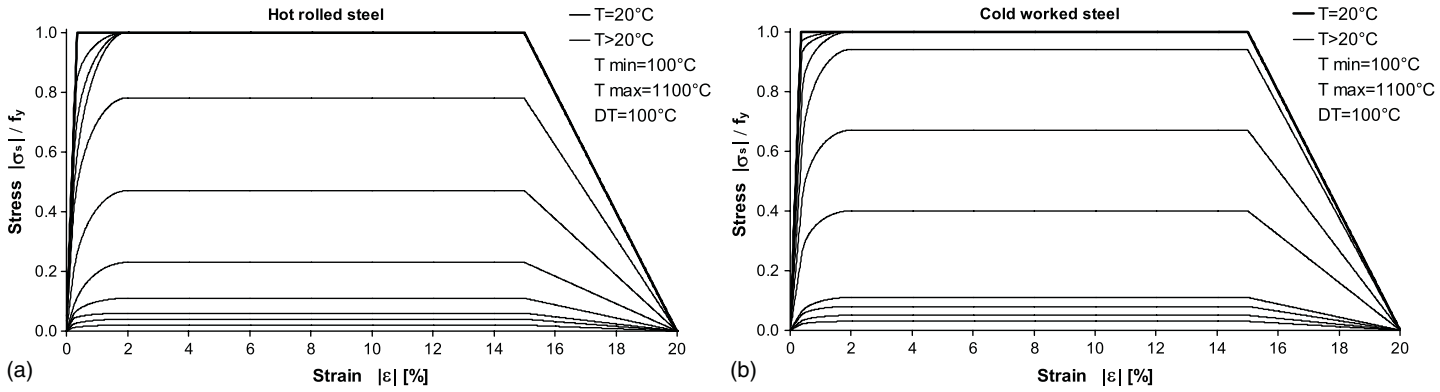

Fig. 5. Temperature-dependent reinforcing steel behavior, stress-strain relationships for (a) hot-rolled steel and (b) cold-worked steel

Steel Behavior

The instantaneous stress-induced strain ε_σ is modeled by using the stress-strain constitutive laws shown in Fig. 5, for both hot-rolled and cold-worked steel (CEN 2004).

The temperature-induced strain ε_T is attributable to the contribution of two terms: thermal strain ε_{th}, and creep strain ε_{cr}, or $\varepsilon_T = \varepsilon_{th} + \varepsilon_{cr}$. According to CEN (2004), the thermal strain ε_{th} is computed by using the following relationships:

$$\varepsilon_{th} = -2.416 \times 10^{-4} + 1.2 \times 10^{-5} T + 0.4 \times 10^{-8} T^2, \quad \text{for } 20°\text{C} \le T \le 750°\text{C} \tag{24a}$$

$$\varepsilon_{th} = 11 \times 10^{-3}, \quad \text{for } 750°\text{C} < T \le 860°\text{C} \tag{24b}$$

$$\varepsilon_{th} = -6.2 \times 10^{-3} + 2 \times 10^{-5} T, \quad \text{for } 860°\text{C} < T \le 1200°\text{C} \tag{24c}$$

The contribution of the creep strain ε_{cr} becomes significant when very sustained high temperatures occur (Rigberth 2000). Such contribution is implicitly included, in an approximate way, in the stress-strain constitutive laws shown in Fig. 5. The accuracy of this approach is generally adequate for structures with relatively low percentage of steel reinforcement (Anderberg 1988).

Time-Variant Structural Analysis under Fire

On the basis of general criteria for nonlinear finite-element analysis of concrete structures (Bontempi et al. 1995; Malerba 1998; Biondini 2004), in the following a finite-element formulation for time-variant structural analysis of framed systems under fire is developed (Biondini and Nero 2006).

Nonlinear Analysis of Deteriorating Reinforced Concrete Cross Sections

The formulation assumes the linearity of concrete strain field and neglects shear failures and bond-slip of reinforcement (Fig. 6). For the cross section x, the vectors of the stress resultants $\mathbf{r} = \mathbf{r}(x,t) = [N \quad M_z \quad M_y]^T$ (axial force N and bending moments M_z and M_y) and of the global strains $\mathbf{e} = \mathbf{e}(x,t) = [\varepsilon_0 \quad \chi_z \quad \chi_y]^T$ (axial strain ε_0 and bending curvatures χ_z and χ_y) are then related, at each time instant t, as follows:

$$\mathbf{r}(x,t) = \mathbf{r}_0(x,t) + \mathbf{r}_T(x,t) = \mathbf{H}(x,t)\mathbf{e}(x,t) \tag{25}$$

where $\mathbf{H} = \mathbf{H}(x,t) = 3 \times 3$ stiffness matrix of the cross section; $\mathbf{r}_0 = \mathbf{r}_0(x,t) = [N_0 \quad M_{z0} \quad M_{y0}]^T$ = vector of the applied stress resultants; and $\mathbf{r}_T = \mathbf{r}_T(x,t) = [N_T \quad M_{zT} \quad M_{yT}]^T$ = vector of the stress resultants equivalent to the temperature-induced effects.

On the basis of the principle of virtual displacements, the stiffness matrix $\mathbf{H} = \mathbf{H}(x,t)$ and the thermal stress vector $\mathbf{r}_T = \mathbf{r}_T(x,t)$ are derived by integration over the area of the composite cross section, or by assembling the contributions of both concrete and steel as follows:

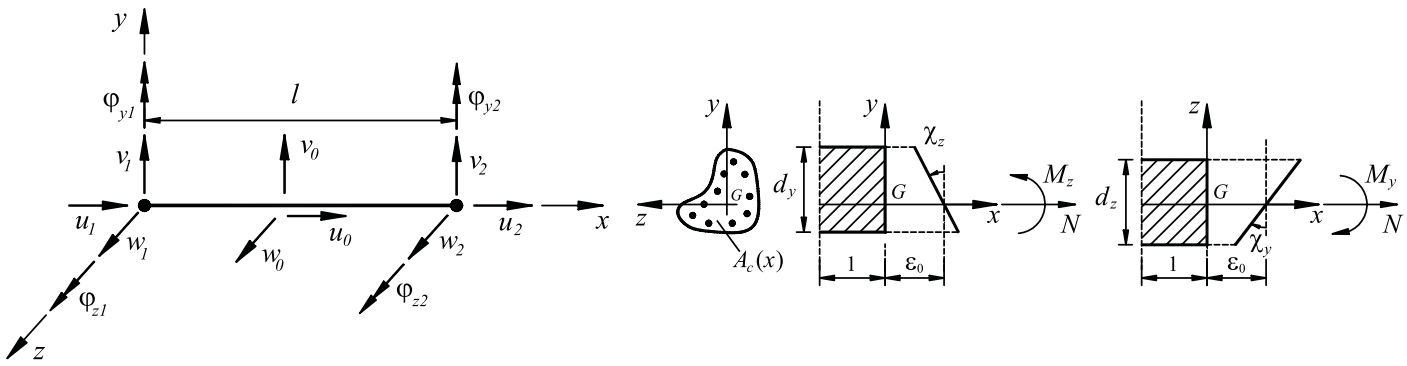

Fig. 6. Main parameters, local reference system, and sign conventions for the finite beam element

$$\mathbf{H}(x,t) = \mathbf{H}_c(x,t) + \mathbf{H}_s(x,t) \tag{26a}$$

$$\mathbf{H}_c(x,t) = \int_{A_c(x)} E_c(x,y,z,t)\mathbf{b}(y,z)^T\mathbf{b}(y,z)dA \tag{26b}$$

$$\mathbf{H}_s(x,t) = \sum_m E_{sm}(x,t)\mathbf{b}_m^T\mathbf{b}_m A_{sm} \tag{26c}$$

$$\mathbf{r}_T(x,t) = \mathbf{r}_{cT}(x,t) + \mathbf{r}_{sT}(x,t) \tag{27a}$$

$$\mathbf{r}_{cT}(x,t) = \int_{A_c(x)} E_c(x,y,z,t)\varepsilon_{cT}(x,y,z,t)\mathbf{b}(y,z)^T dA \tag{27b}$$

$$\mathbf{r}_{sT}(x,t) = \sum_m E_{sm}(x,t)\varepsilon_{sTm}(x,t)\mathbf{b}_m^T A_{sm} \tag{27c}$$

where the symbol "m" refers to the m^{th} reinforcement bar located at (y_m, z_m); $E_c = E_c(x,y,z,t)$ and $E_{sm} = E_{sm}(x,t)$ = generalized moduli of the materials; and $\mathbf{b}(y,z) = [\,1 \quad -y \quad z\,]$. The vectors $\mathbf{r}$ and $\mathbf{e}$ have to be considered as total or incremental quantities depending on the nature of the stiffness matrix $\mathbf{H}$, which depends on the adopted formulation (i.e., secant or tangent) for the generalized moduli of the materials.

Formulation of a Deteriorating Reinforced Concrete Finite Beam Element

The previous cross-sectional formulation is extended to define the characteristics of a reinforced concrete finite beam element for nonlinear analysis of framed structures under fire. The beam element shown in Fig. 6 is considered. The torsional degrees of freedom are not included because torsion is assumed to be uncoupled from axial and bending deformations. The vector of displacements $\mathbf{u} = \mathbf{u}(x,t) = [\,\mathbf{u}_a^T \;|\; \mathbf{u}_b^T]^T = [\,u_0 \;|\; v_0 \quad w_0\,]^T$ and the vector of generalized strains $\mathbf{e} = \mathbf{e}(x,t) = [\,\varepsilon_0 \quad \chi_z \quad \chi_y\,]^T$ can be related to the vector of nodal displacements $\mathbf{s}' = \mathbf{s}'(t) = [\,\mathbf{s}_a^T \;|\; \mathbf{s}_b^T]^T = [\,u_1 \quad u_2 \;|\; v_1 \quad \varphi_{z1} \quad w_1 \quad \varphi_{y1} \quad v_2 \quad \varphi_{z2} \quad w_2 \quad \varphi_{y2}\,]^T$ as follows:

$$\mathbf{u}(x,t) = \mathbf{N}(x)\mathbf{s}'(t) \tag{28}$$

$$\mathbf{e}(x,t) = \mathbf{B}(x)\mathbf{s}'(t) \tag{29}$$

where

$$\mathbf{N}(x) = \begin{bmatrix} \mathbf{N}_a(x) & 0 \\ 0 & \mathbf{N}_b(x) \end{bmatrix} \tag{30}$$

$$\mathbf{B}(x) = \begin{bmatrix} \partial\mathbf{N}_a(x)/\partial x & 0 \\ 0 & \partial^2\mathbf{N}_b(x)/\partial x^2 \end{bmatrix} \tag{31}$$

The axial $\mathbf{N}_a = \mathbf{N}_a(x)$ and bending $\mathbf{N}_b = \mathbf{N}_b(x)$ displacement functions of a linear elastic beam element having uniform cross-sectional stiffness and loaded only at its ends are adopted. On the basis of this assumption, the 10×10 element stiffness matrix $\mathbf{K}' = \mathbf{K}'(t)$ and the nodal force vectors $\mathbf{f}'_p = \mathbf{f}'_p(t)$ and $\mathbf{f}'_T = \mathbf{f}'_T(t)$ equivalent to the applied loads $\mathbf{p} = \mathbf{p}(x,t) = [\,p_{0x} \quad p_{0y} \quad p_{0z}\,]^T$ and to the temperature-induced effects $\mathbf{r}_T = \mathbf{r}_T(x,t)$, respectively, are derived by applying the principle of virtual displacements and then evaluated at each time instant t by integration over the length l of the beam:

$$\mathbf{K}'(t) = \mathbf{K}'_M(t) + \mathbf{K}'_G(t) = \int_0^l \mathbf{B}(x)^T\mathbf{H}(x,t)\mathbf{B}(x)dx + \int_0^l N(x,t)\mathbf{G}(x)^T\mathbf{G}(x)dx \tag{32}$$

$$\mathbf{f}'_p(t) = \int_0^l \mathbf{N}(x)^T\mathbf{p}(x,t)dx \tag{33}$$

$$\mathbf{f}'_T(t) = \int_0^l \mathbf{B}(x)^T\mathbf{r}_T(x,t)dx \tag{34}$$

where $\mathbf{K}'_M = \mathbf{K}'_M(t)$ and $\mathbf{K}'_G = \mathbf{K}'_G(t)$ = material and geometrical contributions to the element stiffness matrix $\mathbf{K}'$, respectively; $N = N(x,t)$ = axial force; and $\mathbf{G} = \mathbf{G}(x)$ = corresponding compatibility matrix:

$$\mathbf{G}(x) = [\,0 \quad \partial\mathbf{N}_b(x)/\partial x\,] \tag{35}$$

The previous quantities need to be evaluated at each time instant by numerical integration. To this aim, without loss of generality and for sake of simplicity, the integration can be effectively based on the three-dimensional grid of the cellular automaton adopted to describe the heat transfer process. To this regard, the grids associated with adjacent beam elements must be properly interconnected to assure the continuity of the thermal flow at their boundaries.

Finally, by assembling the stiffness matrix $\mathbf{K} = \mathbf{K}(t)$ and the vectors of the nodal forces $\mathbf{f} = \mathbf{f}(t)$ in a global reference system, the equilibrium of the whole structure can be expressed as follows:

$$\mathbf{K}(t)\mathbf{s}(t) = \mathbf{f}(t) \tag{36}$$

where $\mathbf{s} = \mathbf{s}(t)$ = global vector of the nodal displacements. As at the cross-sectional level, the vectors $\mathbf{f}$ and $\mathbf{s}$ have to be considered as total or incremental quantities, depending on the nature of the global stiffness matrix $\mathbf{K}$, which depends on the adopted formulation (secant or tangent) for the cross-sectional stiffness matrix $\mathbf{H}$.

Applications

The effectiveness of the proposed methodology is demonstrated by means of applications: two simply supported beams tested in laboratory, a precast beam with elastic restraints, a continuous beam under different fire scenarios, and a frame structure under compartmented fire are analyzed. The time-variant nonlinear analyses are based on the previously introduced thermal and mechanical characteristics of concrete with siliceous aggregates and hot rolled reinforcing steel (CEN 2004). The heat transfer process is described by three-dimensional cellular automata with grid dimension $\Delta x = 13.3$ mm and time step $\Delta t = 0.5$ min.

Simply Supported Beams

The simply supported beams shown in Fig. 7(a) have been exposed to a standardized fire ASTM E119 (ASTM 1976) along their whole length. The beams are subdivided into four finite elements. The numerical results obtained from a time-variant nonlinear analysis are compared with the experimental results of laboratory tests (Hertz 1985). For the beam with rectangular cross section, the results of the numerical analysis are also compared with the results provided by an approximated method formulated by

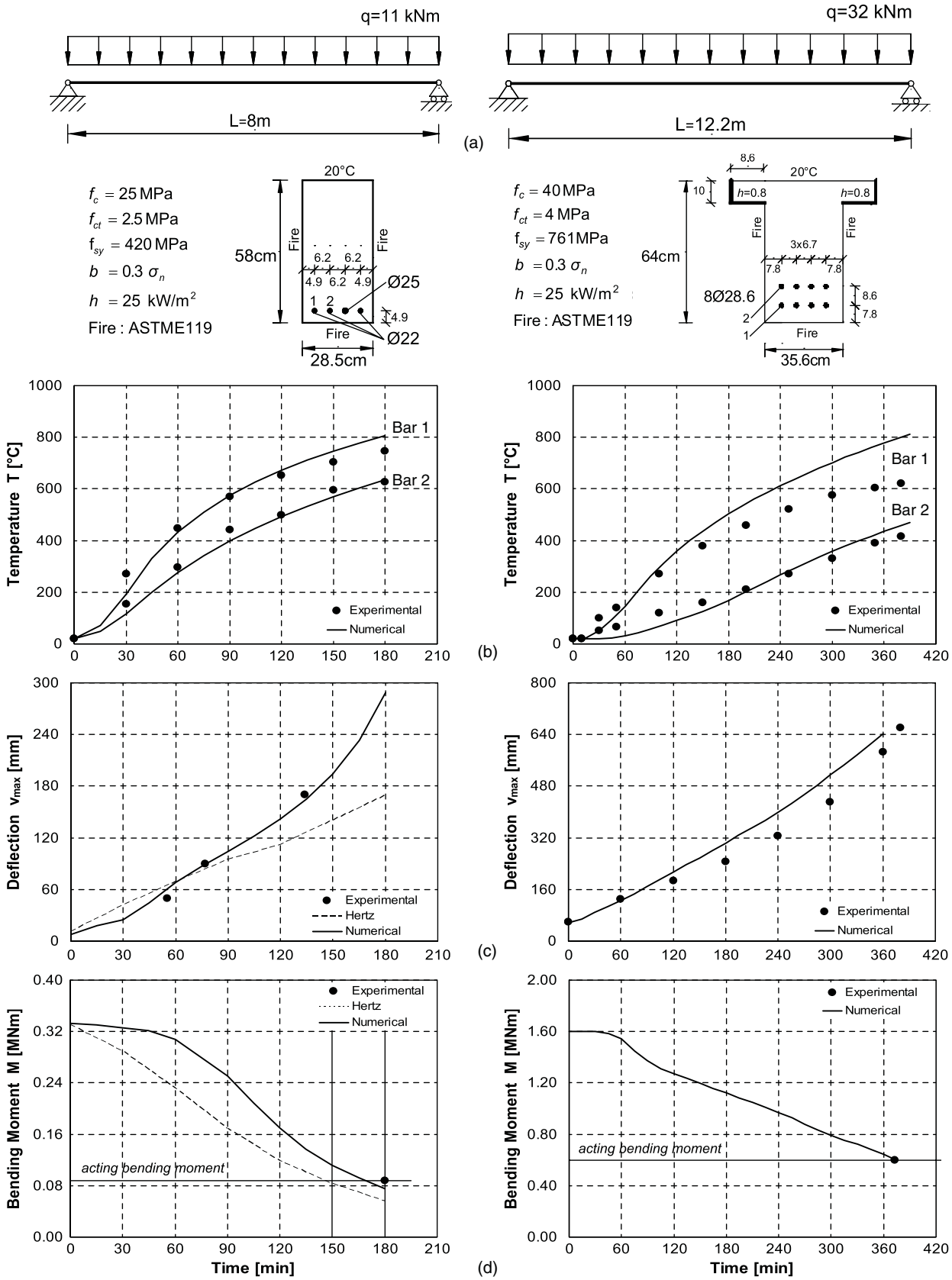

Fig. 7. (a) Simply supported beams with rectangular cross section (left side) and *T* cross section (right side). Comparison between numerical and experimental results in terms of time evolution of (b) temperature in two reinforcing steel bars; (c) maximum deflection; and (d) resistant bending moment versus the maximum acting bending moment

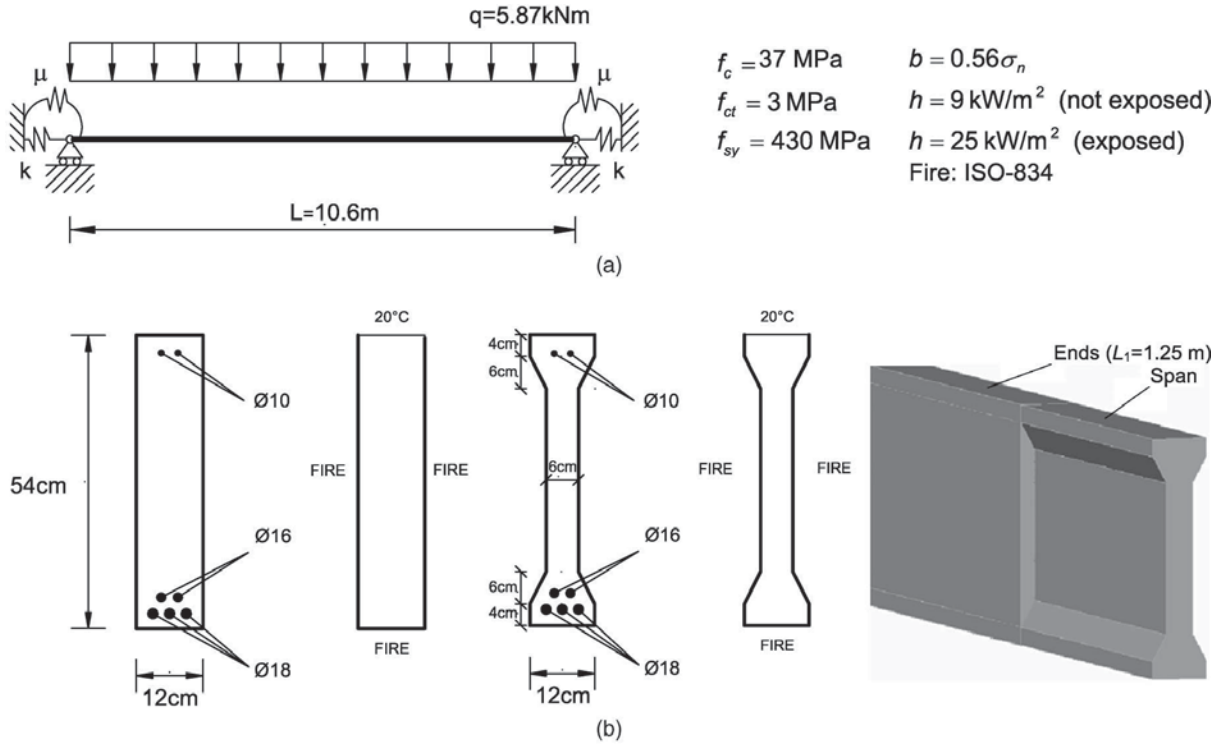

Fig. 8. Precast beam: (a) material properties, geometrical dimensions of the structure; (b) characteristics of the cross sections and fire scenario

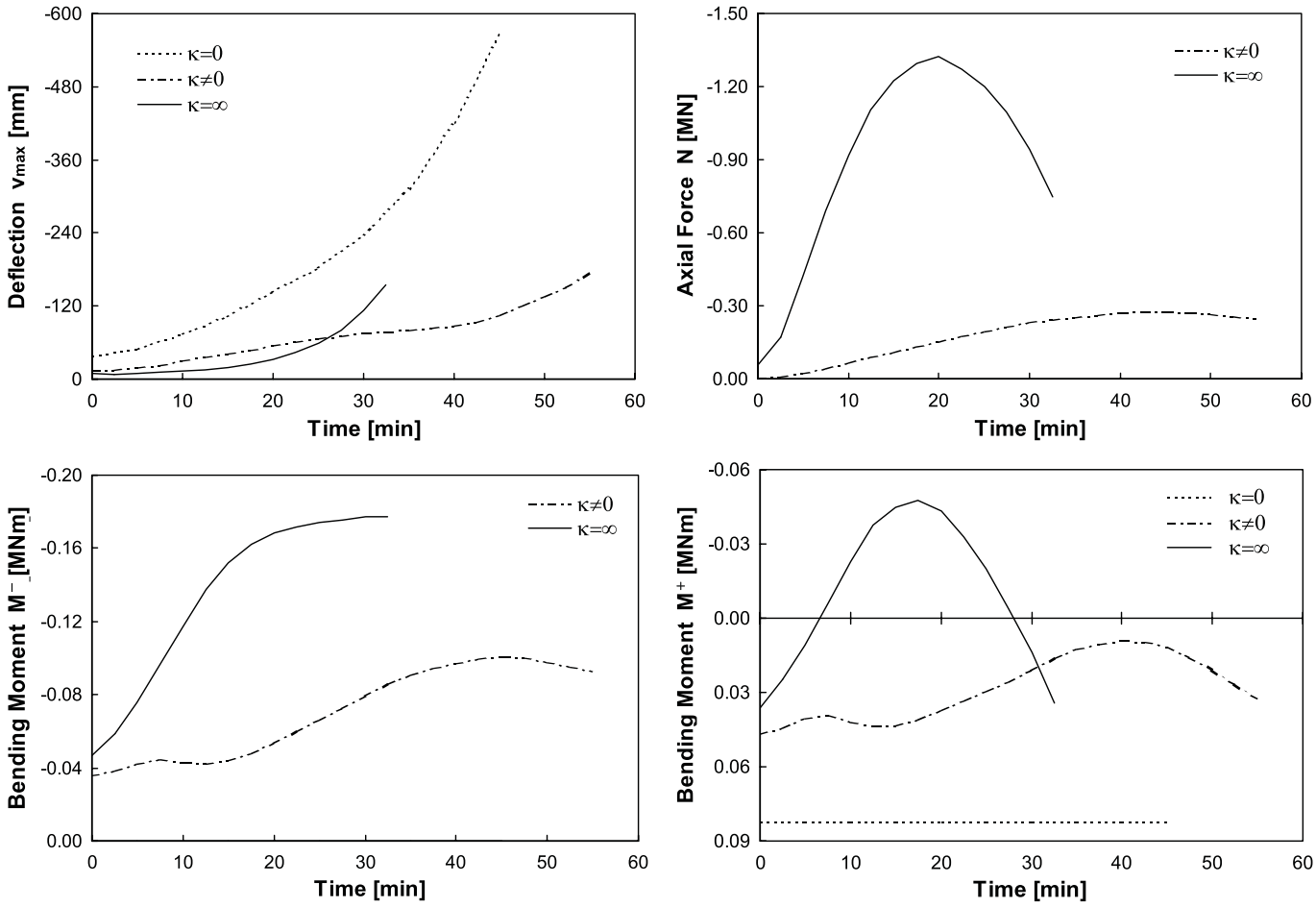

Fig. 9. Precast beam. Time evolution of the structural response in terms of maximum deflection v_{max}, axial force N, and bending moment at the ends M^- and middle span M^+

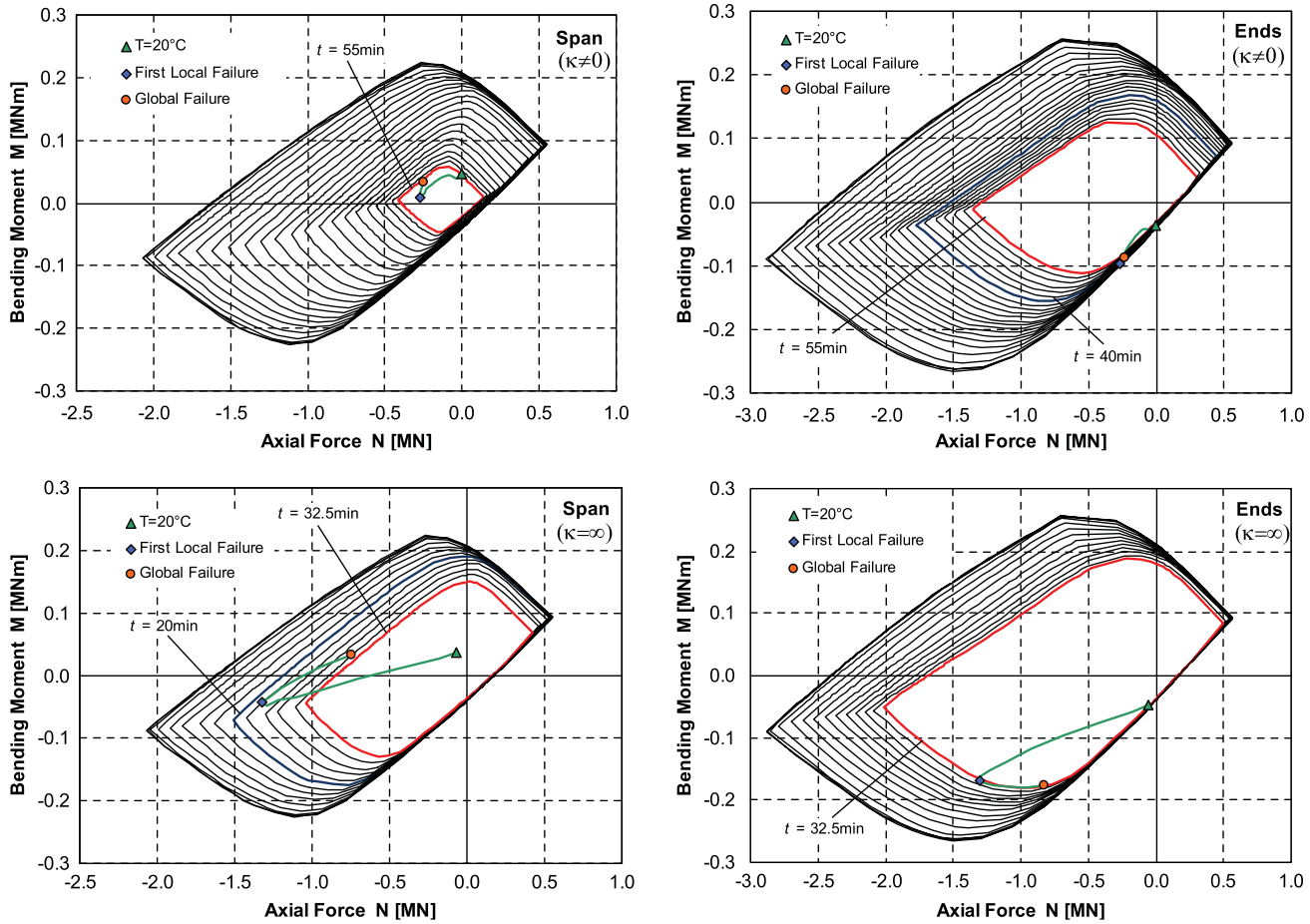

Fig. 10. Precast beam. Comparison between the time evolution of the axial force versus bending moment resistance domains ($\Delta t = 2.5$ min) and the corresponding loading paths

Hertz (Hertz 1985; CEN 2004). These comparisons prove the primacy of the proposed procedure over the approximated method and highlight its effectiveness in reproducing, with high accuracy, the evolution of both the thermal process [Fig. 7(b)] and the structural response [Fig. 7(c)], and in predicting the structural lifetime against fire collapse [Fig. 7(d)].

Precast Beam

The precast beam shown in Fig. 8 is exposed to a standardized fire ISO 834 (ISO 1975) along its whole length. The role of the axial stiffness κ and rotational stiffness μ of the elastic restraints is investigated by considering three separate cases: (1) simply supported beam ($\kappa = \mu = 0$); (2) beam with elastic restraints with stiffness $\kappa = 8.95$ MN/m, and $\mu = 3\kappa = 26.85$ MNm; (3) clamped beam ($\kappa = \mu = \infty$). The beam is subdivided into four finite elements. The results of the time-variant nonlinear analyses are summarized in the diagrams of Figs. 9 and 10. The following remarks can be made:

- The beam deflection increases over time for all the investigated cases, and its maximum value occurs for the simply supported beam during the whole fire event. The deflection of the beam with elastic restraints is initially higher than the deflection of the clamped beam, whereas a reversed tendency arises after 25–30 min (Fig. 9).
- The simply supported beam is axially unloaded. The beam with elastic restraints and the clamped beam are subjected to an axial force which starts from the low initial value induced by the nonlinear coupling with bending behavior and evolves during time according to the corresponding thermal effects (Fig. 9).
- The bending moment diagram of the simply supported beam is constant over time. The time evolution of the bending moment diagram for the beam with elastic restraints and the clamped beam is characterized by remarkable redistribution effects (Fig. 9).
- The most critical cross section is located at the ends for the beam with elastic restraints, and at the middle span for both the simply supported beam and the clamped beam (Fig. 10). For the three investigated cases (1), (2), and (3), the first cross-sectional failure is reached after 45, 40, and 20 min, respectively.
- For the simply supported beam, the local failure of the middle cross section leads to the collapse of the structure. On the contrary, the beam with elastic restraints and the clamped beam can still carry the load after their first local failure, as shown by the comparison between the time evolution of the axial force-bending moment resistance domains and the corresponding loading path in the critical cross sections (Fig. 10). The collapse of these beams is reached after 55 and 32.5 min, respectively.

Continuous Beam

The structural performance of the continuous beam in Fig. 11 is studied with reference to the five scenarios of standardized fire ISO 834 (ISO 1975) described in Fig. 12. The beam is subdivided, in each span, into three finite elements. The results of the time-variant nonlinear analyses are summarized in the diagrams of Figs. 13 and 14. The following remarks can be made:

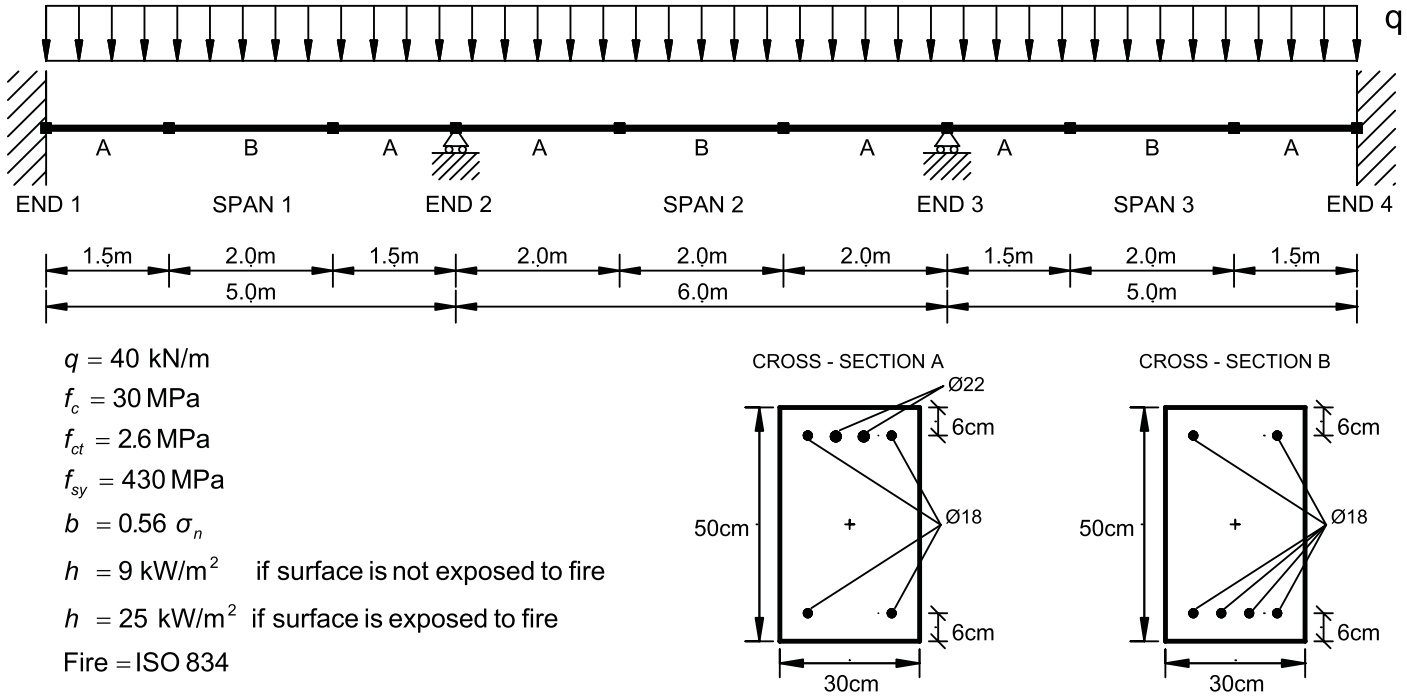

Fig. 11. Continuous beam. Mechanical and thermal properties of the materials, main geometrical dimensions of the structure, distribution and characteristics of the cross sections

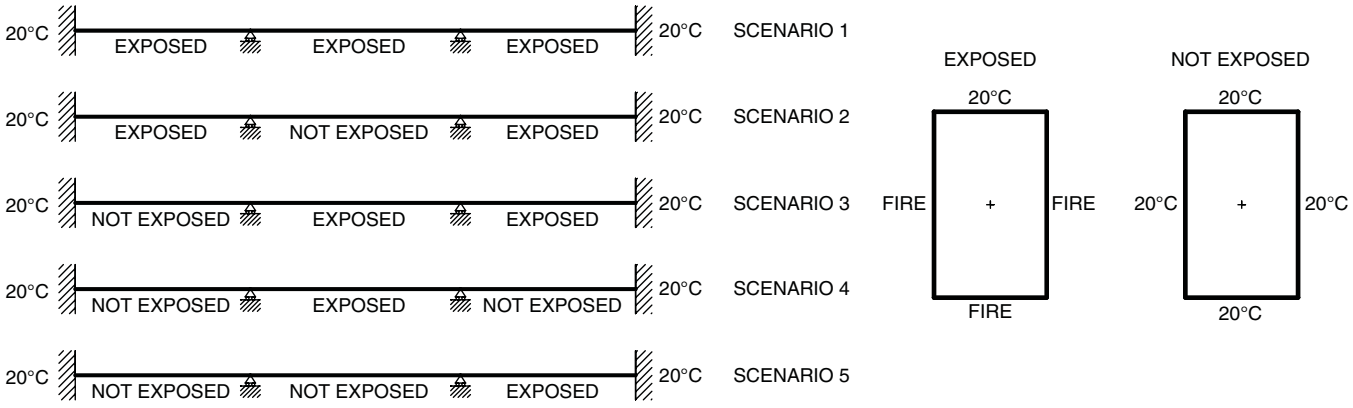

Fig. 12. Fire scenarios for the continuous beam

- The axial force starts from the low initial value induced by the nonlinear coupling with bending behavior and evolves during time in accordance with the corresponding evolution of the axial thermal effects. The maximum value, which clearly depends on the amount of surface exposed to fire, is reached in each scenario after approximately 70–80 min (Fig. 13).
- The time evolution of the bending moment diagram is characterized by remarkable redistribution effects, particularly localized in the zones exposed to fire. In such zones, the bending moment initially tends to increase at the ends and to decrease within the spans, whereas a reversed tendency appears after the first 40–50 min (Fig. 13).
- For Scenarios 1, 3, and 4, the failure of the most critical cross section is reached after 130, 180, and 280 min, respectively. For Scenarios 2 and 5, no failure appears during the first 280 min (Figs. 13 and 14).
- The failed cross section is located at the ends of the central span for Scenario 1, at approximately 15 cm from the left end of the central span for Scenario 3, and at the middle of the central span for Scenario 4 (Fig. 14).
- The comparison between the time evolution of the axial force-bending moment resistance domains and the corresponding loading path in the most critical cross sections shows that, as expected, the margin of safety initially decreases owing to both the decreasing structural resistance and increasing thermal-induced stress contributions. A change in this tendency, however, arises after the first 70–80 min, when the reduction of the axial force begins. As a consequence, in some cross sections, the margin of safety may unexpectedly increase during time depending on the corresponding rate of structural damage (Fig. 14).

The previous comments clearly show that, for redundant structures, the evaluation of fire performance cannot be afforded

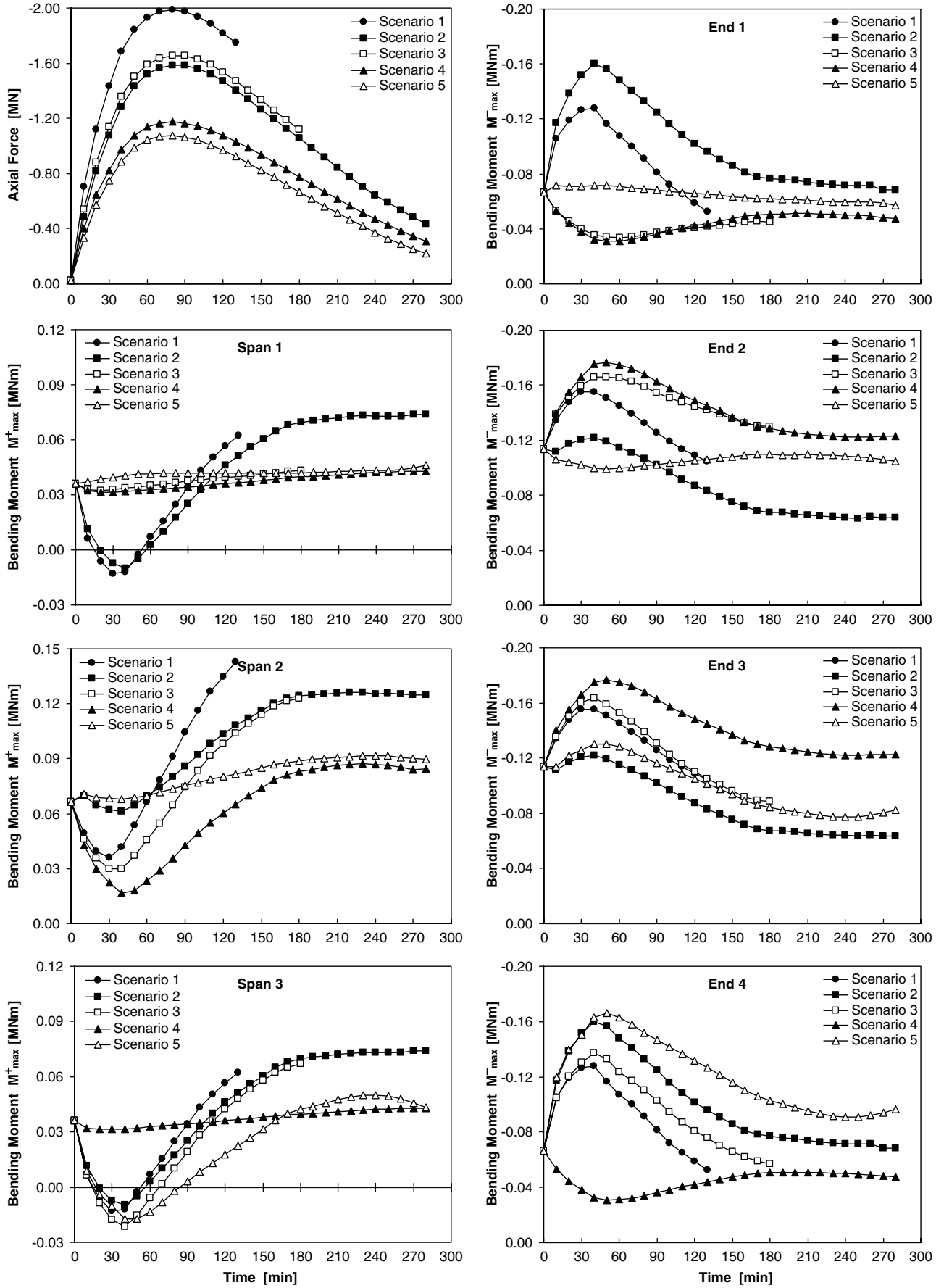

Fig. 13. Continuous beam. Time evolution of the axial force and of the maximum bending moment within the spans ($M^{+}_{\max}$) and at the beam ends ($M^{-}_{\max}$) for the five investigated fire scenarios

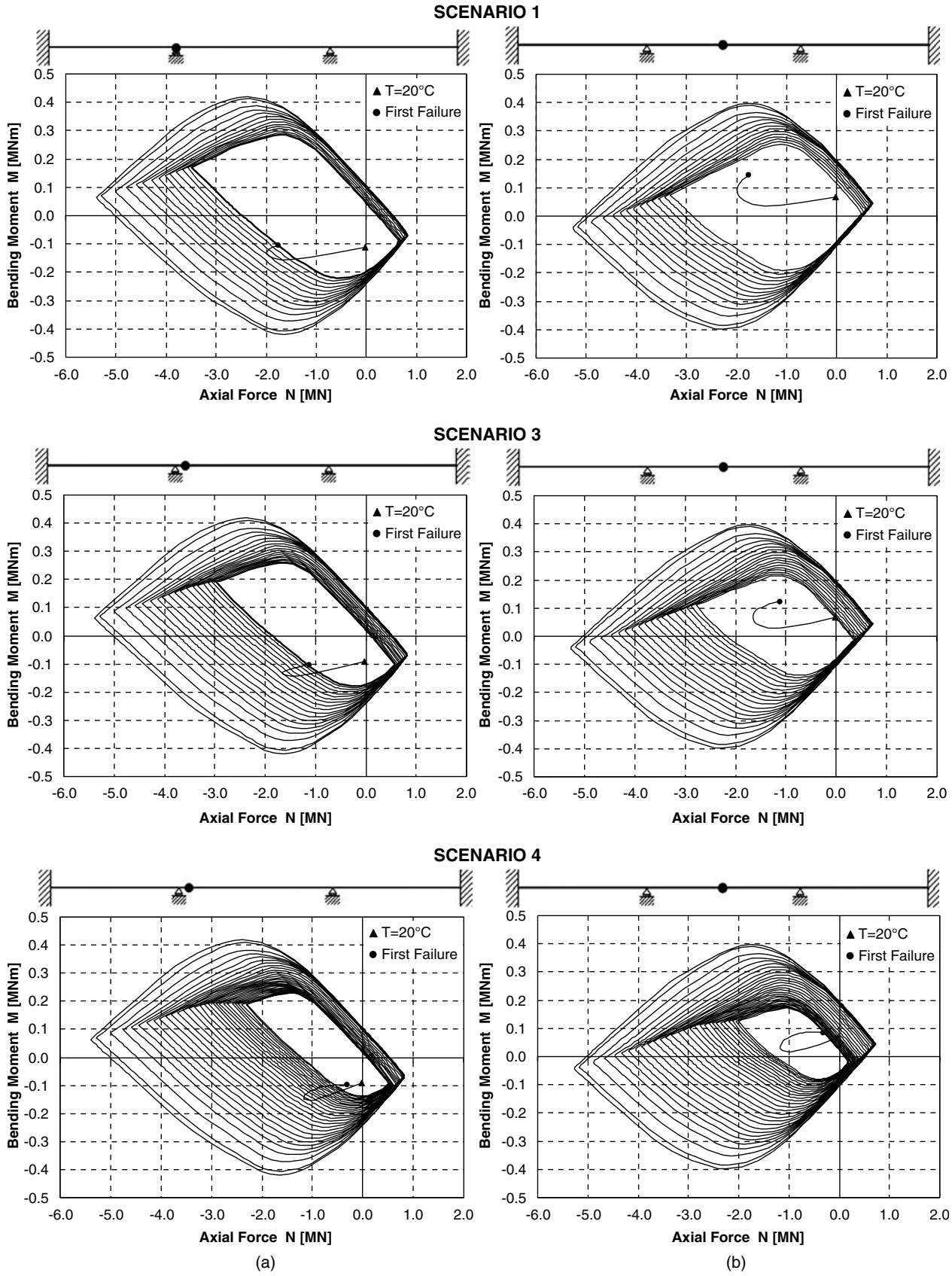

Fig. 14. Continuous beam. Comparison of the time evolution of the axial force versus bending moment resistance domains ($\Delta t = 10$ min) and the corresponding loading paths for Scenarios 1 ($t_{fail} = 130$ min), 3 ($t_{fail} = 180$ min), and 4 ($t_{fail} = 280$ min): (a) cross section at the left end of the central span (Scenario 1), and at approximately 15 cm from such end (Scenarios 3 and 4); (b) cross section at the middle of the central span

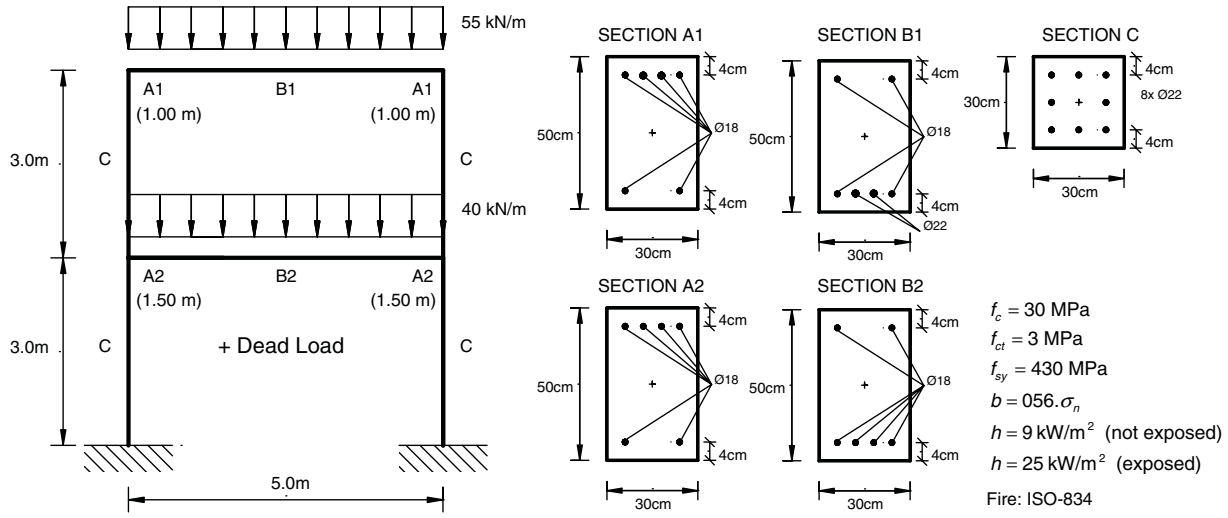

Fig. 15. Frame structure. Material properties, geometrical dimensions of the structure, and characteristics of the cross sections

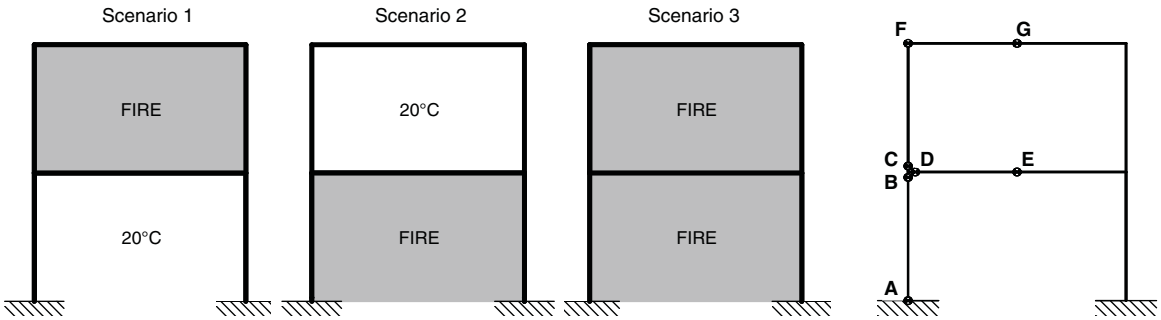

Fig. 16. Fire scenarios for the frame structure

by simply considering the evolution of the thermal-induced damage at the cross-sectional level, but needs to be developed at the structural level by taking into account the actual role played by the structural scheme in the time-variant stress redistribution process. With this regard, the fire performance is strongly dependent on both mechanical and thermal loading history, and the most damaged structural configuration at the end of fire exposition is generally not the most critical.

Frame Structure

The structural performance of the frame structure shown in Fig. 15 is studied with reference to the three scenarios of standardized fire ISO 834 (ISO 1975) described in Fig. 16. The beams subject to fire from the top are exposed on the top face only. The beams subject to fire from the bottom are exposed on the bottom face and the lateral faces. The columns under fire are exposed on the internal face and on the two lateral faces. Each beam and each column are subdivided into four finite elements. The results of the time-variant nonlinear analysis are resumed for all scenarios in the diagrams of Fig. 17. Such diagrams show that the time evolution of the bending moments in the monitored cross sections A–F (Fig. 17) is characterized by remarkable redistribution effects, and the margin of safety strongly depends on the fire scenario. With this regard, for some cross sections, the compartmented fire in Scenarios 1 and 2 is more critical than Scenario 3, characterized by a higher thermal load.

Conclusions

A novel approach to the time-variant nonlinear finite-element analysis of concrete structures exposed to fire has been presented. The main novelty of the proposed formulation is the use of cellular automata to describe the heat conduction, convection, and radiation induced by fire, and to create an effective link between the simulation of the thermal process and the finite-element structural analysis. In this study, the thermal properties of concrete have been assumed to be independent from the stress state, as proposed in CEN (2004). However, it is emphasized that the possibility of accounting for a thermomechanical coupling makes the proposed approach more general than other procedures in which the finite-element analysis is based on temperature maps obtained from a separate thermal fire analysis. In fact, in some cases, the occurrence of stress-related damage phenomena, such as severe cracking, may modify the temperature distribution and lead to a coupling between heat transfer and structural response.

The proposed methodology has been validated through applications: two simply supported beams tested in laboratory, a precast beam with elastic restraints, a continuous beam under different fire scenarios, and a frame structure under compartmented fire, have been analyzed. The results have proven the accuracy of the proposed procedure in reproducing the evolution of both the thermal process and structural response, and in predicting the structural lifetime against fire collapse. Moreover, the results clearly showed that, for redundant structures, the evaluation of fire performance

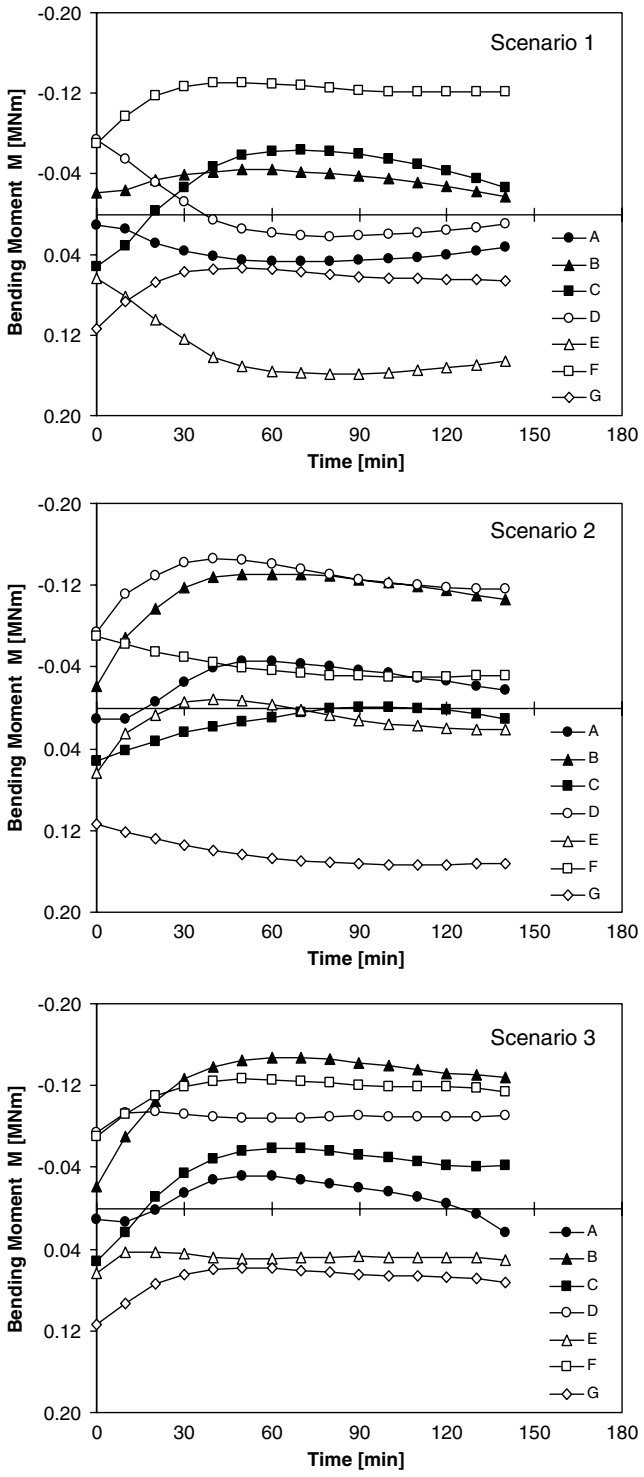

Fig. 17. Frame structure. Time evolution of the bending moment in the monitored cross sections A–F (see Fig. 16) for the three investigated fire scenarios

cannot be afforded by simply considering the evolution of the thermal-induced damage at the cross-sectional level, but needs to be developed at the structural level by taking into account the actual role played by the structural scheme in the time-variant stress redistribution process.

With this regard, it is outlined that the margin of safety depends on the prescribed fire scenario, and that the most critical scenario may not be associated with the maximum thermal load. Moreover, for a prescribed fire scenario, the structural performances are strongly dependent on both mechanical and thermal loading history, and the most damaged structural configuration at the end of fire exposition is generally not the most critical. As a consequence, a reliable assessment of fire safety can be carried out only by means of a time-variant nonlinear analysis that is able to follow the complex loading paths associated with thermal effects. All these aspects can be consistently taken into account by the proposed methodology, which has been proven to be an effective engineering tool in fire analysis of concrete structures.

Acknowledgments

This study has been partially supported by research funds PRIN2005 (prot. 2005082490), Italian Ministry of University and Research—Department of Structural Engineering, Politecnico di Milano.

References

American Concrete Institute (ACI)/Minerals, Metals and Materials Society (TMS). (2007). "Code requirements for determining fire resistance of concrete and masonry construction assemblies." *ACI 216.1-07/TMS-0216-07*, Farmington Hills, MI.

Anderberg, Y. (1988). "Modelling steel behaviour." *Fire Saf. J.*, 13(1), 17–26.

Anderberg, Y. (1991). "SUPER-TEMPCALC." *A commercial and user friendly computer program with automatic fem-generation for temperature analysis of structures exposed to heat*, Fire Safety Design, Lund, Sweden.

Anderberg, Y., and Thelandersson, S. (1976). "Stress and deformation characteristics of concrete at high temperatures. 2. Experimental investigation and material behaviour model." *Bulletin 54*, Lund Institute of Technology, Lund, Sweden.

ASTM. (1976). "Standard methods of fire tests of buildings construction and materials." *E119-76*, West Conshohocken, PA.

Becker, J., and Bresler, B. (1974). "FIRES-RC: A computer program for the fire response of structures—Reinforced concrete frames." *Rep. UCB FRG 74-3*, Fire Research Group, Univ. of California, Berkeley, CA.

Biondini, F. (2004). "A three-dimensional finite beam element for multi-scale damage measure and seismic analysis of concrete structures." *13th World Conf. on Earthquake Engineering (WCEE), Paper No. 2963*, International Association for Earthquake Engineering (IAEE), Tokyo.

Biondini, F., Bontempi, F., Frangopol, D. M., and Malerba, P. G. (2004). "Cellular automata approach to durability analysis of concrete structures in aggressive environments." *J. Struct. Eng.*, 130(11), 1724–1737.

Biondini, F., and Nero, A. (2006). "Nonlinear analysis of concrete structures exposed to fire." *2nd fib Congress, Paper 12-5*, fib, Lausanne, Switzerland.

Biondini, F., and Nero, A. (2007). "Fire performance analysis of concrete structures." *Concrete under Severe Conditions: Environment & Loading (CONSEC'07)*, Metratech, Tours, France.

Bontempi, F., Malerba, P. G., and Romano, L. (1995). "Formulazione diretta secante dell'analisi non lineare di telai in C.A./C.A.P." *Studi e Ricerche*, Milan, Italy, 16, 351–386 (in Italian).

Buchanan, A. H. (2001). *Structural design for fire safety*, Wiley, New York.

Caner, A., Zlatanic, S., and Munfah, N. (2005). "Structural fire performance of concrete and shotcrete tunnel liners." *J. Struct. Eng.*, 131(12), 1920–1925.

European Committee for Standardization (CEN). (2004). "Design of concrete structures—Part1-2: General rules—Structural fire design." *EN 1992-1-2*, Brussels.

Forsén, N. E. (1982). "A theoretical study on the fire resistance of concrete structures." *SINTEF Rep. STF65 A82062*, Cement and Concrete Research Institute, Norwegian Institute of Technology, Trondheim, Norway.

Franssen, J. M. (1987). "Etude du comportement au feu des structures mixtes acier-béton." *Collection des publications de la F.S.A.*, 111, Université de Liège, Liège, Belgium.
Franssen, J. M., Kodur, V. K. R., and Mason, J. (2000). "User's manual for SAFIR. A computer program for analysis of structures submitted to the fire." *Rapport interne SPEC/2000 03*, Univ. of Liège, Ponts et Charpentes, Liège, Belgium.
Hertz, K. (1985). *Analysis of prestressing concrete structures exposed to fire*, Technical Univ. of Denmark, Lyngby, Denmark.
Iding, R., Bresler, B., and Nizamuddin, Z. (1977). "FIRES-T3: A computer program for the fire response of structure-thermal." *Rep. UCB FRG 77-15*, Univ. of California, Berkeley.
Incropera, F. P., and De Witt, D. P. (2002). *Fundamentals of heat and mass transfer*, Wiley, New York.
ISO. (1975). "Fire-resistance tests—Elements of building construction." *834-1975*, Geneva.
Kodur, V. K. R., and Dwaikat, M. B. (2008). "Effect of fire induced spalling on the response of reinforced concrete beams." *Int. J. Concr. Struct. Mater.*, 2(2), 71–81.
Kodur, V. K. R., and Sultan, M. A. (2003). "Effect of temperature on thermal properties of high-strength concrete." *J. Mater. Civ. Eng.*, 15(2), 101–107.
Malerba, P. G., ed. (1998). *Analisi limite e non lineare di strutture in calcestruzzo armato*, International Centre for Mechanical Sciences (CISM), Udine, Italy (in Italian).
Nero, A. (2006). "Analisi non lineare di strutture in calcestruzzo armato esposte ad incendio." Degree thesis, Politecnico di Milano, Milan, Italy (in Italian).
Pichler, C., Lackner, R., and Mang, H. A. (2006). "Safety assessment of concrete tunnel linings under fire load." *J. Struct. Eng.*, 132(6), 961–969.
Rigberth, J. (2000). "Simplified design of fire exposed concrete beams and columns. An evaluation of Eurocode and Swedish building code against advanced computer models." *Rep. 5063*, Dept. of Fire Safety Engineering, Lund Univ., Lund, Sweden.
Schneider, U. (1988). "Concrete at high temperatures—A general review." *Fire Saf. J.*, 13(1), 55–68.
Schneider, U., Schneider, M., and Franssen, J. M. (2008). "Consideration of nonlinear creep strain of siliceous concrete on calculation of mechanical strain under transient temperatures as a function of load history." *5th Int. Conf. on Structures in Fire (SiF'08)*, Singapore, 463–476.
Sterner, E., and Wickström, U. (1990). "TASEF—Temperature analysis of structures exposed to fire." *SP Report 1990:05*, Swedish National Testing and Research Institute, Borås, Sweden.
Wolfram, S. (1994). *Cellular automata and complexity—Collected papers*, Addison-Wesley, Reading, MA.